Source attribution and process analysis for atmospheric mercury in East China simulated by CMAQ-Hg

Jialei Zhu[1,2], Tijian Wang[1], Johannes Bieser[3,4]， Volker Matthias[3]

1. School of Atmospheric Sciences, Nanjing University, Nanjing 210093, China

2. Department of Energy and Environment, Zhejiang Prov. Development Planning & Research Institute, Hangzhou 310012, China

3. Institute of Coastal Research, Helmholtz-Zentrum Geesthacht, Max-Planck-Str. 1, 21502, Geesthacht, Germany

4. National aeronautics and space research center (DRL), Oberpfaffenhofen, 82234, Weßling, Germany

Correspondence to: Tijian Wang (tjwang@nju.edu.cn)

Abstract

The contribution from different emission sources and atmospheric processes to gaseous elemental mercury (GEM), gaseous oxidized mercury (GOM), particulate bound mercury (PBM) and mercury deposition in East China were quantified using the Community Multi-scale Air Quality (CMAQ-Hg) modeling system run with a nested domain. Natural source (NAT) and six categories of anthropogenic mercury sources (ANTH) including cement production (CEM), domestic life (DOM), industrial boilers (IND), metal production (MET), coal-fired power plants (PP) and traffic (TRA) were considered for source apportionment. NAT was responsible for 36.6% of annual averaged GEM concentration which was regarded as the most important source for GEM in spite of obvious seasonal variation. Among ANTH, the influence of MET and PP on GEM were most evident especially in winter. ANTH dominated the variations of GOM and PBM concentration with a contribution of 86.7% and 79.1% respectively. Among ANTH, IND was the largest contributor for

GOM (57.5%) and PBM (34.4%) so that most mercury deposition came from IND. The effect of mercury emitted from out of China was indicated by >30% contribution to GEM concentration and wet deposition. The contribution from nine processes consisting of emissions (EMIS), gas-phase chemical production/loss (CHEM), horizontal advection (HADV), vertical advection (ZADV), horizontal advection (HDIF), vertical diffusion (VDIF), dry deposition (DDEP), cloud processes (CLDS) and aerosol processes (AERO) were calculated for processes analysis with their comparison in urban and non-urban regions of Yangtze River Delta (YRD). EMIS and VDIF affected surface GEM and PBM concentration most and tended to compensate each other all the time in both urban and non-urban areas. However, DDEP was the most important removal process for GOM with 7.3 ng m^{-3} and 2.9 ng m^{-3} reduced in the surface of urban and non-urban areas respectively in a whole day. Diurnal profile variation of processes revealed the transportation of GOM from urban area to non-urban area and the importance of CHEM/AERO in higher altitudes which caused diffusion of GOM downwards to non-urban area partly. Most of the anthropogenic mercury transported and diffused away from urban area by HADV and VDIF and increase mercury concentration in non-urban areas by HADV. Natural emissions only influenced CHEM and AERO more significantly than anthropogenic. Local emission in the YRD contributed 8.5% more to GEM and ~30% more to GOM and PBM in urban areas compared to non-urban areas.

1 Introduction

Mercury (Hg) pollution in the atmosphere attracts increasing concern globally in view of its neurotoxicity and bioaccumulation in along the food chain posing risks to human health (Schroeder and Munthe, 1998; Rolfhus et al., 2003). Atmospheric mercury is divided into three species according to various physical and chemical properties: gaseous elemental mercury (GEM), gaseous oxidized mercury (GOM) and

particulate bound mercury (PBM). GEM is the predominant form (>95%) in atmosphere; it is very stable and well-mixed hemispherically with a long lifetime of 0.5~2 years (Selin et al., 2007). In contrast, GOM and PBM will deposit more rapidly downwind of their emission sources via wet or dry deposition since GOM and PBM have significantly higher reactivity, deposition velocities, and water solubility (Lin and Pehkonen, 1999; Lindberg et al., 2002; Keeler et al., 2005). Accordingly, mercury is a multi-scale pollutant able to be transported at local, regional and long scale distances from the sources and mercury emission speciation has a great impact on processes and spatial distribution of mercury in the atmosphere (Bieser et al., 2014; Quan et al., 2009; Voudouri and Kallos, 2007; Pai et al., 1999).

Mercury is released into the atmosphere from both natural processes and anthropogenic activities. Natural processes such as evasion from soils, water bodies and vegetation just emit GEM with evident seasonal variation (Shetty et al., 2008). The natural sources will also include re-emission of anthropogenic mercury deposited into the environment previously (Gbor et al., 2006). Mercury emissions from anthropogenic sources are mainly from coal combustion, non-ferrous smelters, waste incineration and mining (Streets, et al., 2009). Anthropogenic mercury emissions in Asia are the highest in the world, accounting for about half of the global total (Pacyna et al. 2010). Especially, China is considered as one of the largest and growing source regions due to its rapid economic and industrial growth along with a coal-dominated energy structure (Wu et al., 2006; Wang et al., 2014). Particularly high emissions of mercury in China result in more elevated mercury concentration and larger mercury deposition than background levels in the world even in remote areas such as the Mt. Gongga area (Fu et al., 2008) and Mt. Changbai (Wan et al., 2009). Much more serious atmospheric mercury pollution was detected in Chinese urban sites where total gaseous mercury (TGM) concentrations were a factor of 3~5 higher than those observed in rural areas (Zhu et al., 2012; Chen et al., 2013; Feng et al., 2004, Zhang et

al., 2013). Therefore, improving the understanding of the source-receptor relationships for mercury and providing valuable information on mercury transport, deposition and chemistry within China are urgently needed. Detailed quantitative assessments of the contribution of mercury sources help to determine effective mercury emission control strategies.

Previous publications provided contribution estimates from selected emission sources mostly in the United States (Seigneur et al., 2004; Selin and Jacob, 2008; Lin et al., 2012) and the Great Lakes (Cohen et al., 2004; Holloway et al., 2012) using global and regional chemical transport models. Many studies for Asia focus on the mercury mass outflow caused by the total emission in Asia and its contribution to long range transport (Pan et al., 2010; Lin et al., 2010). Limited source apportionment of mercury pollution in China has been studied by Wang et al. (2014) distinguishing four emission sectors using a global model (GEOS-Chem) in coarse spatial resolution. In addition, few studies focus on diagnostic and process analysis for atmospheric mercury pollution formation and identification of the dominant atmospheric processes for mercury. The mercury version of US EPA's Community Multi-scale Air Quality (CMAQ-Hg) modeling system (Bullock and Brehme, 2002) was widely used to simulate regional atmospheric mercury pollution. Process analysis (PA) embedded in CMAQ can be applied to investigate the relative contribution of the individual processes on simulated concentration. The performance of CMAQ-Hg model in simulating mercury has been evaluated against mercury concentration and deposition measured on surface mostly in US (Holloway et al., 2012; Bullock et al., 2008, 2009; Gbor et al., 2006, 2007).

In this paper, the temporal and spatial distribution of atmospheric mercury and its deposition in 2011 were simulated on a nested domain over East China with grid resolution of 27x27 km² and parent grid resolution of 81x81 km^2 using CMAQ-Hg. The model results were compared to available monitoring data. Seasonal

contributions of all types of mercury emission sources, including natural emissions, cement plants, domestic coal burning, industrial boilers, metal productions, power plants and traffic emissions, to atmospheric mercury concentration and deposition were quantified. The process analysis for atmospheric mercury concentration was used for select urban and non-urban areas. The influence of physical and chemical processes on mercury concentration was examined. This study provides a detailed model study on source apportionment and process analysis of atmospheric mercury in East China.

2 Methods

2.1 Model descriptions

The model used in this study was based on CMAQ v4.6 which has been modified by Bullock and Brehme (2002) and Gbor et al. (2006) to include chemistry, transport and deposition of GEM, GOM and PBM. The model was configured to use the Carbon Bond 5 (CB05) gaseous phase chemistry mechanism (Sarvar et al., 2008) with Euler Backward Iterative (EBI) solver and the AERO4 aerosol mechanism (Binkowski and Roselle, 2002). The CB05 mechanism used here included mercury gaseous reactions with ozone, OH, H_2O_2 and Cl_2 as described by Lin and Tao (2003). The meteorological fields used in CMAQ-Hg were provided by the Weather Research and Forecasting (WRF v3.2) Model. Meteorology-Chemistry Interface Processor (MCIP v3.6) processed the WRF outputs to the CMAQ-Hg model-ready format and dry deposition velocities of GEM and GOM were calculated. The process analysis (PA) technique is an advanced diagnostic method implemented in CMAQ. It provides hourly integrated process rates to quantify the changes in concentration from each of the scientific processes in the mass conservation equations being solved for each mercury species. During this simulation, the contributions from following physical and chemical processes were calculated: emissions of mercury species (EMIS), net

136 gas-phase chemical production/loss (CHEM), horizontal advection (HADV), vertical
137 advection (ZADV), horizontal diffusion (HDIF), vertical diffusion (VDIF), dry
138 deposition (DDEP), cloud processes (CLDS, including cloud attenuation of photolytic
139 rates, convective and non-convective mixing and scavenging by clouds, aqueous-
140 phase chemistry, and wet deposition), aerosol processes (AERO, including
141 thermodynamic equilibrium and dynamics such as homogeneous nucleation,
142 condensation/evaporation, and coagulation) (Liu and Zhang, 2013).
143
144 **2.2 Emission inventory**
145 Both anthropogenic and natural emission inventories of mercury were employed
146 in our simulation with CMAQ-Hg. Emissions from natural sources (NAT) including
147 vegetation, soil surface and water bodies were based on the estimates by Shetty et al.
148 (2008). GEM is the only species emitted from natural sources. Secondary emissions
149 that resulted from deposited mercury transformed to GEM and re-emitted to the
150 atmosphere from soil and water were also considered. Anthropogenic mercury
151 emissions in China were prepared following the approaches of Wang et al. (2014),
152 which were updated to 2007 (Figure 1a). The inventory data were not consistent with
153 our modeling period, but represented the most updated data at the time when this
154 study was conducted. The monthly variation of anthropogenic sources was based on
155 the monthly energy consumption and product yields published in the Chinese
156 yearbook of provincial diversity. The ratios of three mercury species released were
157 varied according to many factors like coal produced in different provinces, mercury
158 content in coal consumed, different boiler types and removal efficiencies and different
159 combinations of atmosphere pollution control devices (Wang et al., 2014). The total
160 anthropogenic mercury sources (ANTH) in China were classified into six categories
161 for source apportionment: (1) emission from cement production (CEM), (2) emission
162 from domestic life (DOM), which includes waste incineration, domestic coal burning

and application of battery and fluorescent lighting, (3) emission from industrial boilers (IND) including boilers used for collective heating in North China during winter, (4) emission from metal production (MET) including zinc smelters, lead smelters, copper smelters, iron production, mercury production and gold production, (5) emissions from coal-fired power plants (PP), which were all treated as large point sources in our simulation, (6) emission from traffic (TRA). Table 1 summarizes the emission inventory for China (land area in the outermost model domain) in 2007. The annual total anthropogenic emissions amount to 638 Mg $year^{-1}$ which was comparable to natural emissions of 551 Mg $year^{-1}$. The average speciation of anthropogenic emissions is as follows: (GEM 49.5%, GOM 38.4%, and PBM 12.1%).

2.3 Model domain and scenarios

The modeling period covers one year from 20 December 2010 to 31 December 2011 including an 11 days spin-up period. Two nested domains were used for CMAQ-Hg model. The first domain (D01, Figure 1a) covers most of China and some other parts of Asia with 85×72 horizontal grid cells at a spatial resolution of 81km×81km. The initial and boundary condition for D01 modeling were extracted from GEOS-Chem global simulation results. The nested domain (D02, Figure 1b) was defined over East China area which is the focus of this study. D02 contains 82×67 horizontal grids with a spatial resolution of 27km×27km. There were 27 vertical layers with a top layer pressure of 100 hPa for both domains. The Yangtze River Delta (YRD) (Figure 1c) is one of the most industrialized and urbanized regions in East China and mercury pollution has become a problem of increasing concern, thus the YRD was chosen for process analysis. Figure 1c showed the land use in the YRD which was divided into three categories of urban, non-urban and water body. A comparison was made of characteristics of processes influencing atmospheric mercury species in urban and non-urban.

Nine emission scenarios in China were considered to understand the relative importance of different emission sources to atmospheric mercury concentration and deposition. The base case (BASE) was run with both natural and all anthropogenic sources mentioned above. Seven sensitivity studies (C1~C7) were designed with one of seven source sectors (i.e. NAT, CEM, DOM, IND, MET, PP and TRA) excluded in each study. In addition, the boundary conditions (BC) were set to zero (C8). Subtracting the results of C1~C8 from the BASE case yields an estimate of mercury associated with these mercury sources.

3 Results and discussion

3.1 Model validation

The spatial distribution of annual average concentration and annual total deposition of GEM, GOM and PBM simulated in BASE are shown in Figure 2. The predicted annual average concentration of GEM, GOM and PBM were in the ranges of 1.8~8.4 ng m^{-3}, 0.015~1.5 ng m^{-3} and 0.017~1.3 ng m^{-3}. On average, GEM constituted 92.8% of the total atmospheric mercury with the contribution going down to a minimum of 58.6% near large anthropogenic sources (Figure 2a). The concentration of GOM and PBM was typically greater at locations of large cities due to the larger anthropogenic emission there and decreased rapidly away from source locations because of their relatively shorter atmospheric lifetimes (Figure 2b,2c). The total mercury deposition was 65.3 μg m^{-2} $year^{-1}$ with 34.3 μg m^{-2} $year^{-1}$ of total dry deposition and 31.0 μg m^{-2} $year^{-1}$ of total wet deposition. The dry deposition of GEM was 4.26 μg m^{-2} $year^{-1}$ on average with the larger deposition in the southern part of D02 due to the larger dry deposition velocity of GEM there (Figure 2d). GOM contributed 28.2 μg m^{-2} $year^{-1}$ to total dry deposition with a range of 2.5~428.4 μg m^{-2} $year^{-1}$, which was the dominant fraction of mercury dry deposition. The distribution of the dry deposition of GOM and PBM resembled the spatial pattern of urban area in

East China as a result of high concentration of GOM and PBM there, especially showing the elevated deposition in the eastern (i.e. YRD) and northern part of D02 (Figure 2e, 2f). The wet deposition was dominated by PBM (56.5%) followed by GOM (43.4%). The distribution of wet deposition was affected by the spatial pattern of concentration and precipitation (Figure 2h, 2i). The wet deposition of GEM was negligible due to its low solubility in water (Figure 2g).

The results from the base case were compared to observations to give a preliminary evaluation of model performance. As long-term mercury measurements in East China are very limited, all available measurement results (listed in Zhu et al., 2012; 2014) in East China were used to assess model skill, of which TGM concentrations were obtained in nine sites, PBM concentrations were obtained in five sites and wet deposition was only observed in Nanjing. The locations of these sites are given in Figure 1b. Although the analysis in the following sections uses the model results for 2011, the same timeframe with observations reported was simulated for model validation. Figure 3 shows the comparison between averaged measurements and CMAQ results during homologous months. Most sites such as Chengshantou (Ci et al., 2011a), Ningbo (Nguyen et al., 2011), Guangzhou (Chen et al., 2013), Jiaxing (Wang et al., 2007), Mt. Dinghu (Chen et al., 2013), Chongming (Dou et al., 2013), Nanjing (Zhu et al., 2012) and Yellow Sea (Ci et al, 2011b), the simulated TGM is quite consistent with observations with relative bias of 4%~28% (Figure 3a). In comparison, modeled TGM concentrations in Pudong were ~51% overestimated. The site in Pudong (Friedli et al., 2011) was located at a costal urban area with less than one month measurement data. The short duration of this measurement and unexpected complex emission and meteorological condition may be responsible for the larger bias. The correlation coefficient between averaged observed and simulated TGM concentration in all sites was 0.85. The model can reproduce the averaged TGM concentration in most areas of East China, but the model results have a smaller

variability especially in urban sites like Nanjing where the standard deviation of simulation result was 4.86 ng m^{-3} lower than that observed. This is expected to be the incapability of the model to capture emission plumes and predict the transient peaks observed in urban sites because of the 27 km grid cell resolution and assumption of instantaneous emission dilution in grid cells (Pongprueksa et al., 2008). As seen in Figure 3b, the model results were also comparable to PBM concentration observed in Nanjing (Zhu et al., 2014), Shanghai (Xiu et al., 2009) and Hefei (Wang, 2010). PBM concentration in Nanjing was underestimated by 60% which may be because the location of the observation site in Nanjing is in the central urban area with much higher particle concentration compared to the averaged concentration in the simulation grid cell. The scarcity of mercury deposition measurement in East China limited the evaluation of model performance for mercury deposition. Our model result agrees reasonably well with mercury wet deposition measurement result in Nanjing site during 9 months in 2011 (Zhu et al., 2014) with 6.3μg m^{-2} underestimated which was caused by 232.8mm (21.8% to total) less precipitation and less PBM concentration in urban area predicted. Overall, our simulation did well in reflecting the levels and deposition of atmospheric mercury in East China and it is suitable for further analysis of source apportionment.

3.2 Source apportionment

3.2.1 Natural Sources (NAT)

Figure 4 and Figure 5 summarize annual and seasonal relative contribution of different source sectors to atmospheric mercury concentration and deposition in East China (land area in D02). Annual total mercury emissions from natural sources were close to those from anthropogenic sources. Because all natural emissions are in the form of GEM, this sector is responsible for 63.6% of the total annual GEM emission in China. The result was that natural sources are the largest contributor to atmospheric

GEM concentration (36.6% in annual average). Due to significant seasonal variation of GEM emission from NAT, the contribution from NAT to GEM varied between 52.2% in summer and 15.0% in winter. NAT was much more important for GEM concentration in summer with a factor of 3.3 to the contribution from ANTH (15.9%). Though GEM was not the key species for mercury deposition, NAT was still an important contribution to wet and dry deposition in summer with 28.5% and 24.3% respectively. That was because of higher emission quantity of NAT and the increased photochemical activities in summer that led to a greater degree of GEM oxidation to GOM and transformation to PBM, which contributed 15.7% of GOM and 24.2% of PBM in summer. In contrast, NAT contributes little to GOM concentration (0.2%), PBM concentration (0.3%) and deposition (2.4% to wet deposition and 1.7% to dry deposition) in winter. Therefore, during winter, ANTH had a much larger impact on atmospheric mercury concentration and deposition. The effect from NAT was decreasing from south to north in mainland of D02, correlating with air temperature. There was no obvious difference between the quantities contributed from NAT to urban and rural areas but the relative contribution to urban areas was lower due to higher emissions and thus concentration and deposition in urban areas.

3.2.2 Cement production (CEM)

In 2011, anthropogenic sources emitted 638 Mg of mercury which was a little more than that from natural sources (551 Mg $year^{-1}$). However, unlike natural sources, mercury from ANTH includes GEM, GOM and PBM. The quantity and speciation of mercury released from six anthropogenic source categories were quite different. This leads to different impacts on the spatial and temporal distribution of atmospheric mercury concentration and deposition.

Total mercury emission from CEM is responsible for 13.5% of the total anthropogenic emissions and ~80% of the mercury from CEM was in the form of

GEM. CEM contributed 6.6% to the total annual GEM concentration which was 23.9% of the total contribution from all anthropogenic sources. The impact on GOM and PBM concentration from CEM was much lower than that of most other anthropogenic sources. As GEM had little impact on mercury deposition, CEM changed wet and dry deposition by only 4.0% and 5.1% respectively. The seasonal variation of the contribution from CEM was negligible because of the production of cement was relatively constant over the whole year. CEM affected the GEM concentration in the eastern coastal area most evidently with up to 20% because of the large emissions from cement plants in the Shandong, Jiangsu and Zhejiang provinces which are responsible for ~26% of the total emissions from CEM in China.

3.2.3 Industrial boilers (IND)

Emissions of total mercury from IND made up 32.9% of all anthropogenic emissions in China. Thus, it is the most important anthropogenic source. Moreover, 70.8% of the total mercury emitted from IND was GOM which makes up 60.8% of the total GOM emissions in China. Moreover, IND was also the largest source of PBM in China. Owing to the large quantity of GOM and PBM which can deposit near the emission sources through dry and wet deposition, IND makes the largest contribution to mercury deposition with 22.3% and 43.6% to annual wet and dry deposition corresponding to 57.5% and 34.4% contribution to annual averaged GOM and PBM concentration. Especially in winter, IND dominated the GOM concentration and mercury dry deposition with the contribution reaching 73.3% and 63.9% respectively as a result of large-scale collective heating in northern China. The measurement by Zhang et al. (2013) also indicated the boilers play an important role in the elevation mercury concentration in winter of rural Beijing.

3.2.4 Power plants (PP)

Emissions from PP were another important sector and they were treated as point sources in the model. GEM and GOM are the main species emitted from PP with a percentage of 68.1% and 30.8% and, in contrast, with only 1.1% of PBM. PP was the smallest contributor (2.5%) to PBM. However, PP was the second largest contributor to GEM and GOM concentration (7.1% and 9.6% respectively) among all anthropogenic sources, although its contribution to GOM concentration was much lower than the largest GOM sources of IND. Emissions from PP were responsible for 5.5% and 9.8% of wet and dry deposition which resulted from significant impact on GOM concentration. There were many larger coal-fired power plants with capacities larger than 1000 MW concentrating in the YRD. Because of this, obviously higher emission intensity from PP led to a much higher influence to atmospheric mercury pollution in the YRD with an annual averaged contribution to TGM of up to 1 ng m^{-3} (>20%).

3.2.5 Metal production (MET)

MET was the largest anthropogenic source of GEM accounting for 31.8% of the anthropogenically emitted GEM. As this sector includes manufacturers and smelters of various iron and non-iron metals, the content of mercury from MET varied greatly depending on production process and the mercury content in raw materials. The speciation factors ranged from 65% to 89% for GEM, 6% to 30% for GOM, and 0% to 17% for PBM. Overall, MET contributed 8.4%, 8.2% and 5.0% to GEM, GOM and PBM concentration and was responsible for 4.7% and 7.2% of the annual wet and dry deposition in East China respectively. Although MET was distributed widely in East China, the effects of emissions from MET were greatest in Shaanxi Province due to high mercury concentrations in zinc ore and some small scale plants with poor mercury control devices (Wu et al., 2012).

3.2.6 Domestic life (DOM) and traffic emission (TRA)

Emissions from DOM (6.3%) and TRA (4.4%) were the small fraction of anthropogenic sources. They both hardly affected GEM concentration with a contribution of less than 1% and had little influence on GOM concentration (4.4% from DOM and 1.8% from TRA). However, over 50% of total PBM emission came from DOM and TRA and they increased the annual averaged PBM concentration by 24.4% and 8.0% respectively. As PBM was the main component in mercury wet deposition, DOM was the most important anthropogenic contributor (9.1%) to wet deposition except IND (22.3%). In contrast, DOM and TRA were the two smallest contributors to mercury dry deposition with the proportion of 4.8% and 1.9% because GOM was the dominant contributor to mercury dry deposition. The distribution of emissions from TRA was very heterogeneous with the majority emitted in large cities. In spite of the lower total emissions from TRA, the impacts on PBM concentration and deposition were much higher in and around the province capitals and other large cities by a factor of 2~20 compared to rural areas.

3.2.7 Long-range transport (BC)

The impacts of boundary conditions (BC) were also significant for mercury pollution in East China, which indicates the contribution of mercury emission from other source regions. GEM can be transported far beyond the regions where it is emitted and it is hardly deposited. Therefore, GEM in the global mercury pool affected the concentration in China evidently suggested by our simulation result with up to 34.3% annual averaged GEM concentration from BC. However, BC have little effect on GOM concentration with a contribution of only 8.6% because of its relatively short lifetime. The contribution to GEM concentration from BC was largest in winter while the contribution was least to GOM concentration then because of relatively weaker emissions of GEM and stronger emission of GOM in China during

379 winter. BC influenced the annual averaged PBM concentration by 13.3% due to the
380 low dry deposition velocity of fine size PBM. As PBM was removed mainly by wet
381 deposition, BC contributed 32.3% to annual wet deposition of mercury in China. In
382 comparison, only 15.4% of annual dry deposition was linked to BC owing to the small
383 contribution to GOM. Lin et al. (2012) estimated that 89.1% of mercury dry
384 deposition and 93.2% of mercury wet deposition in contiguous US regions are caused
385 by global sources, which is much higher than that ratio estimated for East China in
386 this study. One of the reasons for this is the much higher local anthropogenic emission
387 of mercury in China. Moreover, the anthropogenic sources out of China were not
388 defined accurately. The underestimate of emission sources from other countries
389 would lead to less contribution from BC to East China.
390
391 **3.3 Process analysis**
392 Figure 2 depicts the simulated concentration and deposition of mercury species
393 during 2011 in East China, which indicated that the Yangtze River Delta (YRD) is one
394 of most polluted areas with high mercury concentration and deposition. Also, the
395 YRD is one of the most active areas of human activity in China. Therefore, the YRD
396 area which is shown in Figure 1c was chosen to study the influence of each physical
397 and chemical process implemented in CMAQ on atmospheric mercury. The area was
398 divided into urban, non-urban and water body depends on the predominant land use.
399 The area with urban coefficient of land use more than 10% was defined as urban area
400 in this study. Comparisons of the contribution of each process to urban and non-urban
401 mercury concentrations were studied.
402
403 **3.3.1 Controlling processes**
404 The annual averaged diurnal variations of the contribution from nine processes
405 which included horizontal advection (HADV), vertical advection (ZADV), horizontal

406 diffusion (HDIF), vertical diffusion (VDIF), emissions (EMIS), dry deposition
407 (DDEP), cloud physics and scavenging (CLDS) and gas and aerosol phase chemistry
408 (CHEM/AERO) to the concentration of GEM, GOM and PBM in the near-surface
409 layer (the first layer in model which was about 50m) in urban and non-urban areas of
410 the YRD are shown in Figure 6. The results indicate that two major processes
411 dominate surface GEM concentration, namely EMIS and VDIF and their
412 contributions were comparable in urban and non-urban area (Figure 6a). The
413 contributions of EMIS and VDIF to the change of GEM concentration were
414 noticeably temporally variable with much higher values during mid-day. Their
415 contribution in midnight were >5 times larger than those at night and they tended to
416 compensate each other all of the time. The effect of EMIS extended gradually in
417 daytime along with the increase of temperature and solar radiation which led to higher
418 emission from NAT. Anthropogenic activity and production are more active during
419 day time which raised the emissions of mercury, especially in urban area. EMIS was
420 the only processes with a positive contribution to GEM concentration in urban areas
421 with annual average of 1.26 ng m^{-3} h^{-1} and other processes all played the opposite
422 role. However, HADV and ZADV could contribute to both gain and loss of GEM in
423 non-urban area throughout the day. Advection processes had more significant
424 influence on surface GEM concentration during the evening and early morning in
425 both urban and non-urban areas but ZADV had the opposite effect with a positive
426 influence in non-urban and a negative in urban areas at night possibly because of the
427 strong heat island circulation. Processes of DDEP and CLDS made small
428 contributions to the loss of GEM. On average, they reduced the concentration of GEM
429 by about 0.8 ng m^{-3} per day in urban and non-urban areas.
430 Unlike GEM, the contributions from different processes on surface GOM and
431 PBM concentrations were much lower in non-urban than that in urban areas due to
432 lower emissions of GOM and PBM in non-urban areas (Figure 6b, 6c). EMIS and

VDIF were also the dominant processes to change surface GOM and PBM concentrations similar to GEM. However, DDEP and CLDS were two additional dominant processes influencing GOM and PBM because of higher dry deposition velocity and reactivity of GOM and PBM. Particularly for GOM, DDEP was the most important removal process with the surface concentration of 7.3 ng m^{-3} and 2.9 ng m^{-3} reduced in urban and non-urban area respectively in a whole day. Local dry deposition of GOM was about 48% of local emissions in urban areas while that in non-urban areas was 42% larger than local emissions which was affected by the emissions from nearby urban areas. In addition, VDIF could contribute to gain of surface GOM in non-urban area in most hours, which indicated higher GOM concentrations in the free troposphere. Figure 7 displays annual averaged diurnal profiles of the variation of HADV, VDIF, CHEM and AERO below 2 km. HADV played almost opposite roles in changing GOM concentration within the boundary layer in urban and non-urban areas (Figure 7a, b), but the trend of temporal variation and magnitude of contribution were about the same. It further indicated the transport of GOM from urban to non-urban areas which was the main source of GOM in upper air of non-urban areas. The contribution of VDIF to the GOM concentration is displayed in Figure 7c. More horizontally advected GOM aloft was mixed downwards to ground levels along with the increase of boundary layer height with the largest contribution of ~0.06 ng m^{-3} h^{-1} at noon, which was why the contribution from VDIF was positive in the surface layer and negative in higher altitudes. CHEM was another contributor to the accumulation of GOM as well as AERO to PBM in the upper air, though CHEM and AERO seemed to be negligible to change GOM and PBM concentration in the surface layer. Figure 7d-7f show that the contributions of CHEM and AERO were much higher in the upper layers than that at surface especially around noon since most of mercury chemical reactions rely on solar radiation. CHEM and AERO are the most important processes to transform GEM to GOM and PBM in the atmosphere. Within 2 km upon non-urban

areas, the column concentration of GOM was increased by 41.9 ng m^{-2} owing to the transformation of GEM through CHEM and the column concentration of PBM was enhanced by 29.1 ng m^{-2} through AERO in a whole day. The enhancements of GOM and PBM through CHEM and AERO in urban area was about 13% less than that in non-urban area. A combination of HADV, ZADV, VDIF, DDEP and CLDS tended to cancel out the gain of PBM from EMIS and AERO in urban area. In spite of most decrease from VDIF in urban area, the other four processes also make 21% contribution to remove surface PBM. However, both of HADV and ZADV transported PBM to surface layer in non-urban areas. The strongest increase of surface PBM occurred in the afternoon at 16-18 h due to higher emission rates of DOM and TRA which were the most important source for PBM while most of the decrease occurred in the morning between 9-11 h because the VDIF process was most effective then. In urban areas, the contribution from DDEP to PBM was 20% less than that from CLDS. In comparison, DDEP made 57% more contribution than CLDS to the loss of surface PBM in non-urban areas. The contribution from HDIF was negligible for all of GEM, GOM and PBM concentrations.

3.3.2 Impacts of sources on processes

Different mercury emission sources had different influences on processes due to the different distribution and intensity of emission sources. The contributions of natural sources and various anthropogenic sources to GEM processes in urban and non-urban areas of the YRD are compared in Figure 8. Various anthropogenic sources, especially CEM and PP, were the main sources leading to GEM advection out of urban areas with 0.077 ng m^{-3} h^{-1} by HADV while natural sources mainly caused GEM to be horizontally transported away from non-urban areas with 0.021 ng m^{-3} h^{-1} (Figure 8a). ANTH made a similar contribution to DDEP and CHEM of GEM in both non-urban and urban areas. In comparison, natural sources affected DDEP and CHEM

of GEM >110% more in non-urban than urban areas though emission from NAT in non-urban area only 38% more than that in urban area (Figure 8d, 8e). Conversely, NAT caused comparable loss of GEM by VDIF in both areas and ANTH influenced VDIF of GEM in urban areas much more evidently (Figure 8c). In the YRD, emissions of GEM mostly came from CEM and PP which contributed locally to GEM concentrations with 0.32 and 0.27 ng m^{-3} h^{-1} in urban areas. More than 80% of the GEM emissions in non-urban areas were emitted by natural sources (Figure 8b). Totally, local emission in the YRD contributed 37.2% to the annual averaged GEM concentration in non-urban and 45.7% to that in urban areas.

Local emissions in the YRD were the primary source for GOM and PBM concentration with a contribution of 74.8% (92.9%) to GOM concentration and 44.0% (66.0%) to PBM concentration in non-urban (urban) area respectively. As GOM and PBM were the main constituents of mercury deposition, local emission in the YRD contributed 65.1% (88.7%) to the annual mercury dry deposition and 37.3% (56.2%) to mercury wet deposition in non-urban (urban) of YRD area. Obviously, local emissions have a larger influence on mercury concentration and deposition in urban areas. However, local emissions also were the most important factor for mercury pollution in non-urban areas. Figure 9 and Figure 10 show the contribution from different sources on the various processes of GOM and PBM in two areas. Natural sources only affected CHEM and AERO especially in non-urban areas significantly compared to anthropogenic sources (Figure 9e, 10e). IND was the largest contributor to all processes of GOM except for CHEM (Figure 9) while DOM contributed most to all processes of PBM besides of AERO (Figure 10). All anthropogenic sources increased the outflow of GOM and PBM from urban areas and enhanced the inflow into non-urban areas. Moreover, the quantity of inflow in non-urban areas was directly proportional to the outflow in urban areas which also indicates the influence of urban emissions on mercury pollution in non-urban areas via HADV (Figure 9a,

10a). Figure 9c depicts that the effects of PP to VDIF of GOM were opposite to those of other anthropogenic sources. Emissions from PP enhanced the surface GOM concentration by VDIF, which was because the emissions from PP was mostly in the free troposphere and formed a large concentration center there. Most of the GOM in higher altitudes would be diffused to the surface in local urban areas and others would be transported to non-urban areas and then increase surface GOM concentration there by VDIF. Due to the limited emissions of PBM from PP, the influence on VDIF of PBM from PP was negligible (Figure 10c).

4. Conclusion

The simulation of atmospheric mercury in East China was conducted using CMAQ-Hg with a grid resolution in a nested domain of 27km to study source apportionment and process analysis. An updated mercury emission inventory for 2007 with anthropogenic emission of 638 Mg $year^{-1}$ in China as well as emissions from natural sources of 551 Mg $year^{-1}$ was used for this simulation. The base model results were consistent with the measurements of atmospheric mercury including the concentration of TGM and PBM as well as the wet deposition in most sites of East China.

Model results for source apportionment showed that natural emissions are the most important source for GEM concentration in East China with a contribution of 36.6%. However natural sources were less important in winter than anthropogenic sources due to significant seasonal variation of emissions. Among the anthropogenic sources, metal production (MET) and power plants (PP) were largest contributors to GEM. For GOM and PBM, anthropogenic sources dominated the variation of concentration with a contribution of 86.7% and 79.1% to the annual averaged concentrations. Industrial sources (IND) were responsible for 57.5% of the GOM concentration on average with the highest influence during winter time. IND also

541 contributed significantly to PBM together with domestic sources (DOM) and they
542 accounted for 58.8% of annual averaged PBM. 42.7% and 62.4% of wet and dry
543 deposition of mercury in East China came from anthropogenic sources respectively.
544 Because of the large contribution to GOM and PBM, IND led to the most mercury
545 deposition. Natural sources amounted a quarter of wet and dry deposition in summer
546 owing to higher emissions and the increased photochemical oxidation to GOM and
547 transformation to PBM during this season. The impact of mercury emitted from
548 outside of China was also significant for mercury pollution in East China. This was
549 indicated by a contribution of more than 30% from the model boundary conditions
550 (BC) to GEM concentration and wet deposition.

551 The influence of atmospheric processes on mercury concentration in the near-
552 surface layer was analyzed in urban and non-urban areas of the YRD. Emissions and
553 vertical diffusion affected surface GEM and PBM concentration most and tended to
554 compensate each other all the time in both urban and non-urban areas. However, dry
555 deposition was the most important removal process for GOM with 7.3 ng m^{-3} and 2.9
556 ng m^{-3} deposited in urban and non-urban areas respectively on an average day. The
557 variation of diurnal profiles of different processes (i.e.: HADV, VDIF, CHEM and
558 AERO) inside the planetary boundary layer indicated the transport of mercury from
559 urban to non-urban areas. Moreover, it was found that gas phase and aerosol
560 chemistry (CHEM and AERO) have a large impact on GOM and PBM concentrations
561 inside the free troposphere. The high concentration of GOM aloft in non-urban areas
562 could be diffused downwards by VDIF. Most of anthropogenic sources caused
563 mercury to be transported and diffused away from urban areas by HADV and VDIF
564 and increased the concentration in non-urban areas by HADV. In contrast, emissions
565 from power plants (PP) enhanced surface GOM concentration by VDIF because
566 emission from PP led to a large concentration center in upper air. Natural sources only
567 influenced CHEM and AERO in both areas more significantly than anthropogenic

568 sources. Local emission in the YRD contributed 8.5% more to GEM and ~30% more
569 to GOM and PBM in urban than those in non-urban areas
570

Acknowledgements

This work was supported by the National Key Basic Research Development Program of China (2014CB441203,2011CB403406), the Specialized Research Fund for the Doctoral Program of Higher Education of China (20110091110010) and a project funded by the Priority Academic Program Development of Jiangsu Higher Education Institutions (PAPD). Thanks to Prof. Shuxiao Wang and Dr. Long Wang from Tsinghua University for providing mercury emission data.

578 **Reference**

579 Bieser, J., De Simone, F., Gencarelli, C., Geyer, B., Hedgecock, I., Matthias, V.,
580 Travnikov, O. and Weigelt, A.: A diagnostic evaluation of modeled mercury wet
581 depositions in Europe using atmospheric speciated high-resolution observations,
582 Environ. Sci. Pollut. Res., 21(16), 9995-10012, 2014.

583 Binkowski, F. S. and Roselle, S. J.: Models-3 Community Multiscale Air Quality
584 (CMAQ) model aerosol component 1. Model description, J. Geophys. Res., 108,
585 4183–4201, doi:10.1029/2001JD001409, 2003.

586 Bullock, O. R. J. and Brehme, K. A.: Atmospheric mercury simulation using the
587 CMAQ model: formulation description and analysis of wet deposition results,
588 Atmos. Environ., 36, 2135–2146, doi:10.1016/S1352-2310(02)00220-0, 2002.

589 Bullock, O. R., Atkinson, D., Braverman, T., Civerolo, K., Dastoor, A., Davignon, D.,
590 Ku, J.-Y., Lohman, K., Myers, T. C., Park, R. J., Seigneur, C., Selin, N. E., Sistla,
591 G., and Vijayaraghavan, K.: An analysis of simulated wet deposition of mercury
592 from the North American Mercury Model Intercomparison Study, J. Geophys.
593 Res., 114, 1–12, doi:10.1029/2008JD011224, 2009.

594 Bullock, O. R., Atkinson, D., Braverman, T., Civerolo, K., Dastoor, A., Davignon, D.,
595 Ku, J.-Y., Lohman, K., Myers, T. C., Park, R. J., Seigneur, C., Selin, N. E., Sistla,
596 G., and Vijayaraghavan, K.: The North American Mercury Model
597 Intercomparison Study (NAMMIS): Study description and model-to-model
598 comparisons, J. Geophys. Res., 113, 1–17, doi:10.1029/2008JD009803, 2008.

599 Chen, L., Liu, M., Xu, Z., Fan, R., Tao, J., Chen, D., Zhang, D., Xie, D. and Sun, J:
600 Variation Trends and Influencing Factors of Total Gaseous Mercury Inthe Pearl
601 River Delta-A Highly Industrialised Region in South Chinainfluenced by
602 Seasonal Monsoons. Atmos. Environ., 77, 757-766, 2013.

603 Ci, Z.J., Zhang, X.S., Wang, Z.W. and Niu, Z.C.: Atmospheric gaseous elemental
604 mercury (GEM) over a coastal/rural site downwind of East China: temporal

variation and long-range transport. Atmos. Environ., 45, 2480-2487, 2011a.

Ci, Z.J., Zhang, X.S., Wang, Z.W., Niu, Z.C., Diao, X.Y. and Wang, S.W.: Distribution and air-sea exchange of mercury (Hg) in the Yellow Sea. Atmos. Chem. Phys. 11, 2881-2892, 2011b.

Cohen, M., Artz, R., Draxler, R., Miller, P., Poissant, L., Niemi, D., Ratté, D., Deslauriers, M., Duval, R., Laurin, R., Slotnick. J., Nettesheim, T., and McDonald, J.: Modeling the atmospheric transport and deposition of mercury to the Great Lakes, Environ. Res., 95, 247-265, 2004.

Dou, H., Wang, S., Wang, L., Zhang, L. and Hao, J.: Characteristics of Total Gaseous Mercury Concentrations at a Rural Site of Yangtze Delta，China. Environ. Sci. (in Chinese), 34, 1-7, 2013.

Feng, X., Shang, L., Wang, S., Tang, S., and Zheng, W.: Temporal variation of total gaseous mercury in the air of Guiyang, China, J. Geophys. Res., 109, D03303, doi:10.1029/2003JD004159, 2004.

Friedli, H.R., Arellano, A.F., Geng, and F., Pan, L.: Measurements of atmospheric mercury in Shanghai during September 2009, Atmos. Chem. Phys., 11, 3781-3788, 2011.

Fu, X. W., Feng, X. B., Zhu, W. Z., Wang, S. F., and Lu, J.: Total gaseous mercury concentrations in ambient air in the eastern slope of Mt. Gongga, South-Eastern fringe of the Tibetan plateau. China. Atmos. Environ. 42, 970–979, 2008

Gbor, P. K., Wen, D., Meng, F., Yang, F., Zhang, B. and Sloan, J. J.: Improved model for mercury emission, transport and deposition, Atmos. Environ.. 40, 973-983, 2006.

Gbor, P., Wen, D., Meng, F., Yang, F., and Sloan, J.: Modeling of mercury emission, transport and deposition in North America, Atmos. Environ., 41, 1135–1149, doi:10.1016/j.atmosenv.2006.10.005, 2007.

Holloway, T., Viogt, C., Morton, J., Spak, S. N., Rutter, A. P. and Schauer, J. J.: An

632 assessment of atmospheric mercury in the Community Multiscale Air Quality
633 (CMAQ) model at an urban site and a rural site in the Great Lakes Region of
634 North America, Atmos. Chem. Phys., 12, 7117-7133, 2012.
635 Keeler, G. J., Gratz, L. E., and Al-Wali, K.: Long-term Atmospheric Mercury Wet
636 Deposition at Underhill, Vermont, Ecotoxicology, 14, 71–83, 2005.
637 Lin, C. J. and Pehkonen, S. O.: The chemistry of atmospheric mercury: A review,
638 Atmos. Environ., 33, 2067–2079, 1999.
639 Lin, C. J., Pan, L., Steets, D. G., Shetty, S. K., Jang, C., Feng, X., Chu, H. W. and Ho,
640 T. C.: Estimating mercury emission outflow from East Asia using CMAQ-Hg,
641 Atmos. Chem. Phys., 10, 1853-1864, 2010.
642 Lin, C. J., Shetty, S. K., Pan, L., Pongprueksa, P., Jang, C. and Chu, H.: Source
643 attribution for mercury deposition in the contiguous United States: Regional
644 difference and seasonal variation, J. Air Waste Manage, 62(1), 52-63, 2012.
645 Lin, X. and Tao, Y.: A numerical modelling study on regional mercury budget for
646 eastern North America, Atmos. Chem. Phys., 3, 535-548, 2003.
647 Lindberg, S. E., Brooks, S., Lin, C. J., Scott, K. J., Landis, M. S., Stevens, R. K.,
648 Goodsite, M., and Richter, A.: Dynamic oxidation of gaseous mercury in the
649 arctic troposphere at polar sunrise, Environ. Sci. Technol., 36, 1245–1256,
650 doi:10.1021/es0111941, 2002.
651 Liu, X. and Zhang, Y: Understanding of the formation mechanisms of ozone and
652 particulate matter at a fine scale over the southeastern U.S.: Process analyses and
653 responses to future-year emissions, Atmos. Environ., 74, 259-276, 2013.
654 Nguyen, D., Kim, J., Shim, S. and Zhang, X.: Ground and shipboard measurements of
655 atmospheric gaseous elemental mercury over the Yellow Sea region during
656 2007–2008, Atmos. Environ., 41, 253-260, 2011.
657 Pacyna, E.G., Pacyna, J.M., Sundseth, K., Munthe, J., Kindbom, K., Wilson, S.,
658 Steenhuisen, F., and Maxson, P.: Global emission of mercury to the atmosphere

659 from anthropogenic sources in 2005 and projections to 2020. Atmospheric
660 Environment 44, 2487-2499, 2010.
661 Pai, P., Karamchandani, P., Seigneur, C. and Allan M.: Sensitivity of simulated
662 atmospheric mercury concentrations and deposition to model input parameters, J.
663 Geophys. Res., 104, 13855-13868, 1999.
664 Pan, L., Lin, C. J., Carmichael, G. R., Streets, D. G., Tang , Y., Woo, J. H., Shetty, S.
665 K., Chu, H. W., Ho, T. C., Friedli, H. R. and Feng, X.: Study of atmospheric
666 mercury budget in East Asia using STEM-Hg modeling system, Sci. Total
667 Environ., 408, 3277-3291, 2010.
668 Pongprueksa, P., Lin, C. J., Lindberg, S.E., Jang, C., Braverman, T., Russell Bullock
669 Jr., O., Ho, T. C. and Chu, H. W.: Scientific uncertainties in atmospheric mercury
670 models III: boundary and initial conditions, model grid resolution, and Hg(II)
671 reduction mechanism. Atmos. Environ., 42(8), 1828–1845, 2008.
672 Quan, J., Zhang, Q. and Zhang, X.: Emission of Hg from coal consumption in China
673 and its summertime deposition calculated by CMAQ-Hg, Terr. Atmos. Ocean.
674 Sci., 20,325-331, 2009.
675 Rolfhus, K.R., Sakamoto, H.E., Cleckner, L.B., Stoor, R.W., Babiarz, C.L., Back,
676 R.C., Manolopoulos, H., Hurley, J.P.: Distribution and fluxes of total and methyl
677 mercury in Lake Superior. Environ. Sci. and Technol., 37, 865–872, 2003.
678 Sarwar, G., Luecken, D., Yarwood, G., Whitten, G. Z., and Carter, W. P. L.: Impact of
679 an Updated Carbon Bond Mechanism on Predictions from the CMAQ Modeling
680 System: Preliminary Assessment, J. Appl. Meteorol. Clim., 47, 3–14,
681 doi:10.1175/2007JAMC1393.1, 2008.
682 Schroeder, W.H., and Munthe, J.: Atmospheric mercury—an overview. Atmos.
683 Environ. 32, 809–822, 1998.
684 Seigneur, C., Vijayaraghavan, K., Lohman, K., Karamchandani, P., and Scott, C.:
685 Global Source Attribution for Mercury Deposition in the United States, Environ.

686 Sci. Technol., 38, 555-569, 2004.
687 Selin, N. E., and Jacob, D. J.: Seasonal and spatial patterns of mercury wet deposition
688 in the United States: constraints on the contribution from North American
689 anthropogenic sources, Atmos. Environ., 42 (21), 5193–5204, 2008.
690 Selin, N. E., Jacob, D. J., Park, R. J., Yantosca, R. M., Strode, S., Jaegle, L., and Jaffe,
691 D.: Chemical cycling and deposition of atmospheric mercury: Global constraints
692 from observations, J. Geophys. Res.-Atmos., 112, D02308,
693 doi:10.1029/2006jd007450, 2007.
694 Shetty, S., Lin, C., Streets, D., and Jang, C.: Model estimate of mercury emission
695 from natural sources in East Asia, 42, 8674-8685, 2008.
696 Streets, D. G., Zhang, Q. and Wu, Y.: Projections of global mercury emissions in
697 2050, Environ. Sci. Technol., 36(8), 2983-2988, 2009.
698 Wan, Q., Feng, X.B., Lu, J.L., Zheng, W., Song, X.J., Li, P., Han, S.J., and Xu, H.:
699 Atmospheric mercury in Changbai Mountain area, northeastern China I: the
700 season distribution pattern of total gaseous mercury and its potential sources.
701 Environ. Res. 109, 201–206, 2009.
702 Wang, L., Wang, S., Zhang, L., Wang, Y., Zhang, Y., Nielsen, C., McElroy, M. B. and
703 Hao, J.: Source apportionment of atmospheric mercury pollution in China using
704 the GEOS-Chem model, Environ. Pollut., 190, 166-175, 2014.
705 Wang, Y.: The speciation, levels and potential impacted factors of atmospheric
706 mercury in Hefei, Central China (in Chinese), University of Science and
707 Technology of China, 2010.
708 Wang, S.X., Zhang, L., Wang, L., Wu, Q.R., Wang, F. Y. and Hao, J. M.: A review of
709 atmospheric mercury emissions, pollution and control in China. Front. Environ.
710 Sci. Eng., DOI: 10.1007/s11783-014-0673-x, 2014.
711 Wang, Z.W., Chen, Z.S., Duan, N., and Zhang, X.S.: Gaseous elemental mercury
712 concentration in atmosphere at urban and remote sites in China. J. Environ. Sci.

19, 176–180, 2007.

Wu, Q.R., Wang , S.X., Zhang, L., Song, J.X., Yang, H. and Meng, Y.: Update of mercury emissions from China's primary zinc, lead and copper smelters, 2000-2010, Atmos. Chem. Phys., 12, 11153-11163, 2012.

Wu, Y., Wang, S., Streets, D. G., Hao., J., Chan, M. and Jiang, J.: Trends in Anthropogenic Mercury Emissions in China from 1995 to 2003. Environ. Sci. Technol., 40, 5312-5318, 2006.

Xiu, G., Cail, J., Zhang, W., Zhang, D., Bueler, A., Lee, S., Shen, Y., Xu, L., Hunag, X., Zhang, P.: Speciated mercury in size-fractionated particles in Shanghai ambient air. Atmos. Environ., 43, 3145-3154, 2009.

Zhang, L., Wang, S. X., Wang, L. and Hao, J. M.: Atmospheric mercury concentration and chemical speciation at a rural site in Beijing, China: implications of mercury emission sources. Atmos. Chem. Phys., 13, 10505–10516, 2013.

Zhu, J., Wang, T., Talbot, R., Mao, H., Hall, C. B., Yang, X., Fu, C., Zhuang, B., Li, S., Han, Y. and Huang, X.: Characteristics of atmospheric Total Gaseous Mercury (TGM) observed in urban Nanjing, China. Atmos. Chem. Phys., 12, 12103–12118, 2012.

Zhu, J., Wang, T., Talbot, R., Mao, H., Yang, X., Fu, C., Sun, J, Zhuang, B., Li, S., Han, Y. and Xie, M.: Characteristics of atmospheric mercury deposition and size-fractionated particulate mercury in urban Nanjing, China. Atmos. Chem. Phys., 12, 2233–2244, 2014.

735 Table 1 Summary of mercury emissions in the model domain 1

	GEM(Mg/year)	GOM(Mg/year)	TPM(Mg/year)	Total(Mg/year)
Natural	551	0	0	551
Anthropogenic	316	245	77	638
CEM	69.0	12.9	4.3	86.2
DOM	6.4	9.2	24.7	40.3
IND	34.1	149.0	27.2	210.3
MET	100.6	30.1	5.3	136.0
PP	84.2	38.1	1.3	123.6
TRA	8.1	5.9	14.0	28.0
Total	867	245	77	1189

736

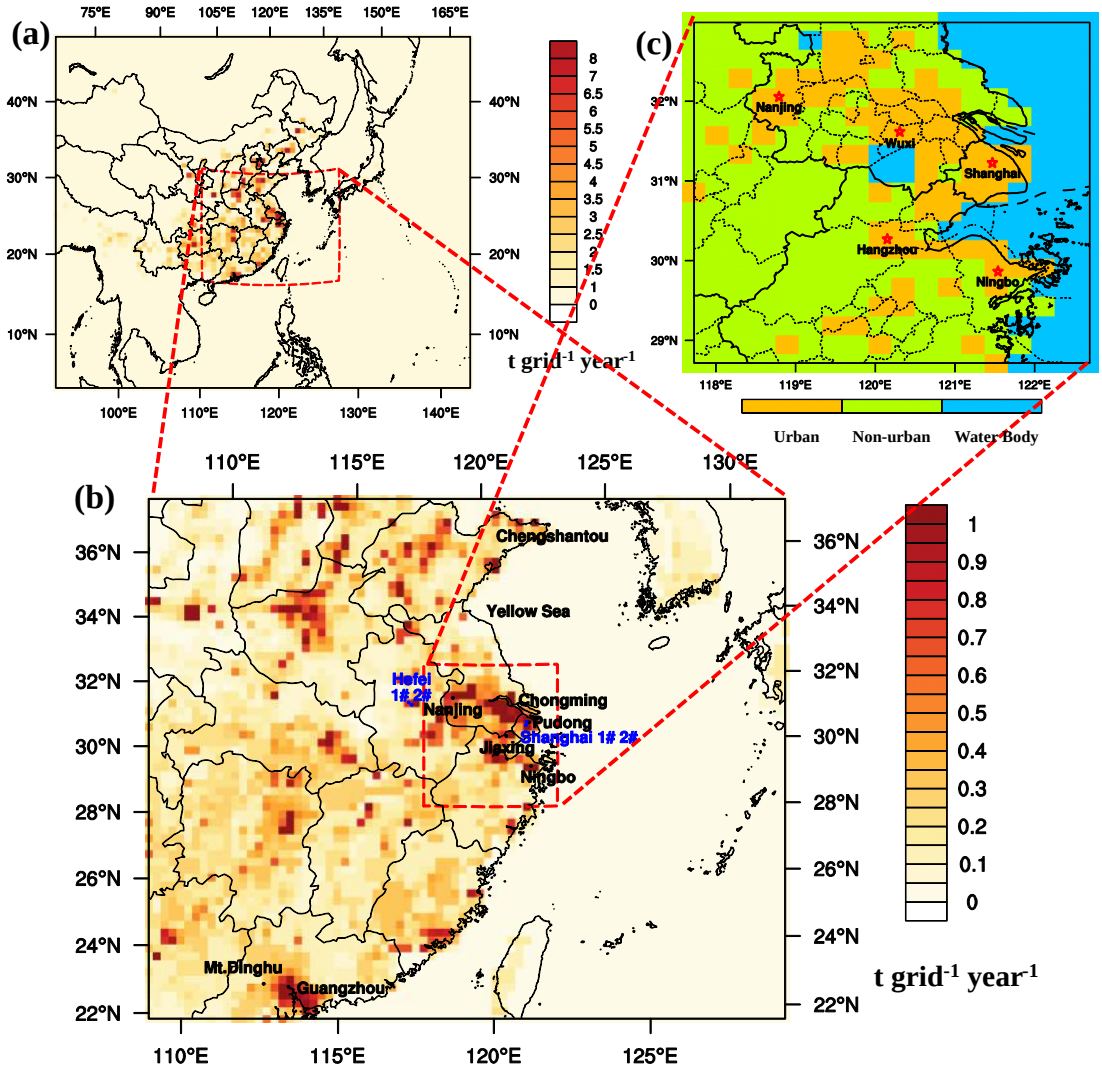

737

738 Figure 1 Model domain (a) Domain 1 with annual total mercury emission (b) Domain

739 2 with annual total mercury emission (c) Yangtze River Delta (YRD) area with land

740 use category

741

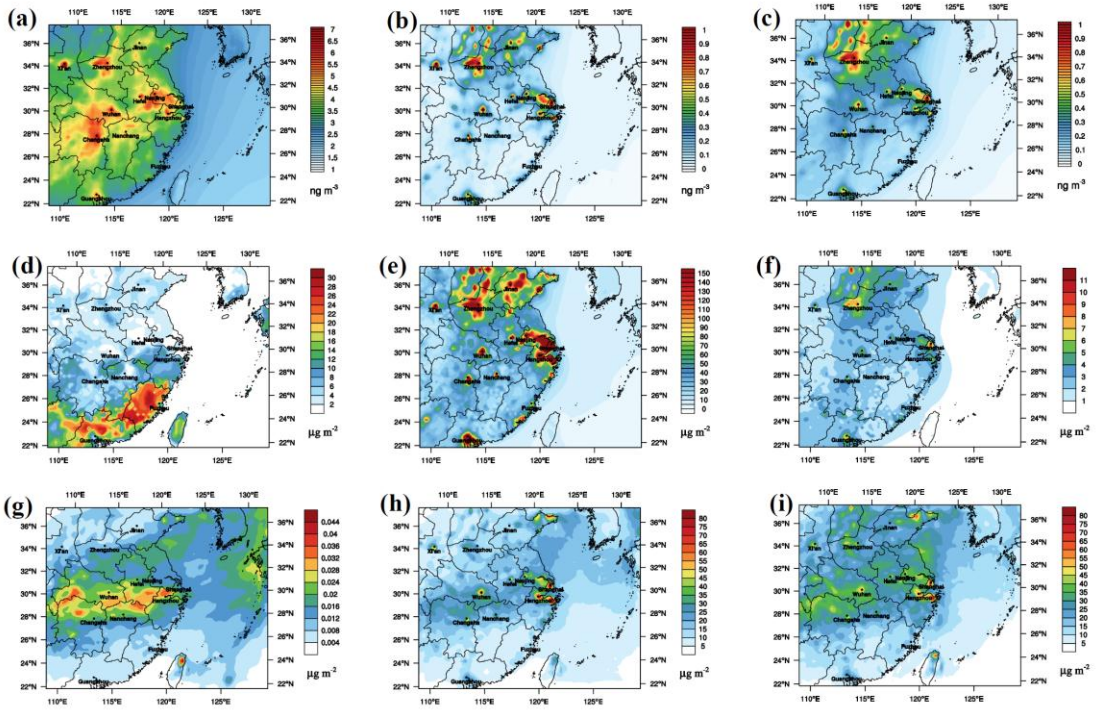

Figure 2 Simulated annual average concentration of (a) GEM, (b) GOM and (c) PBM, annual dry deposition of (d) GEM, (e) GOM and (f) PBM and dry deposition of (g) GEM, (h) GOM and (i) PBM in East China in 2011

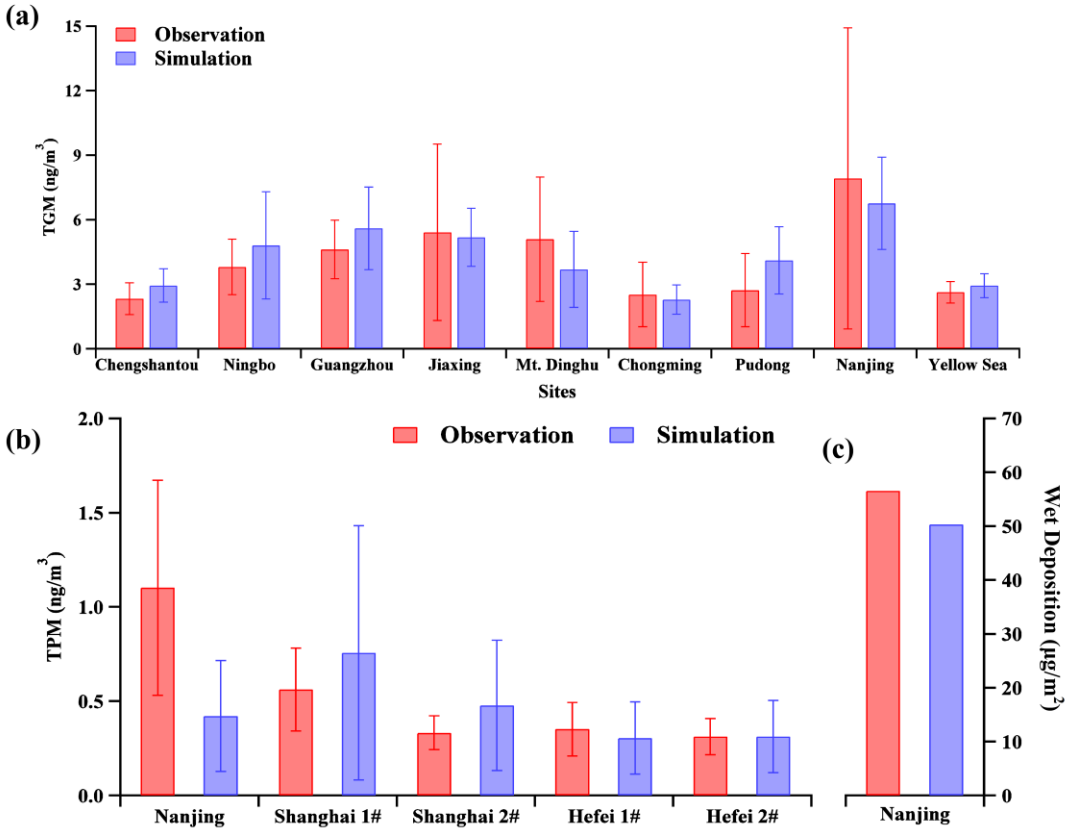

Figure 3 Comparison between simulated results and measurements in sites for (a) TGM concentration, (b) PBM concentration and (c) wet deposition.

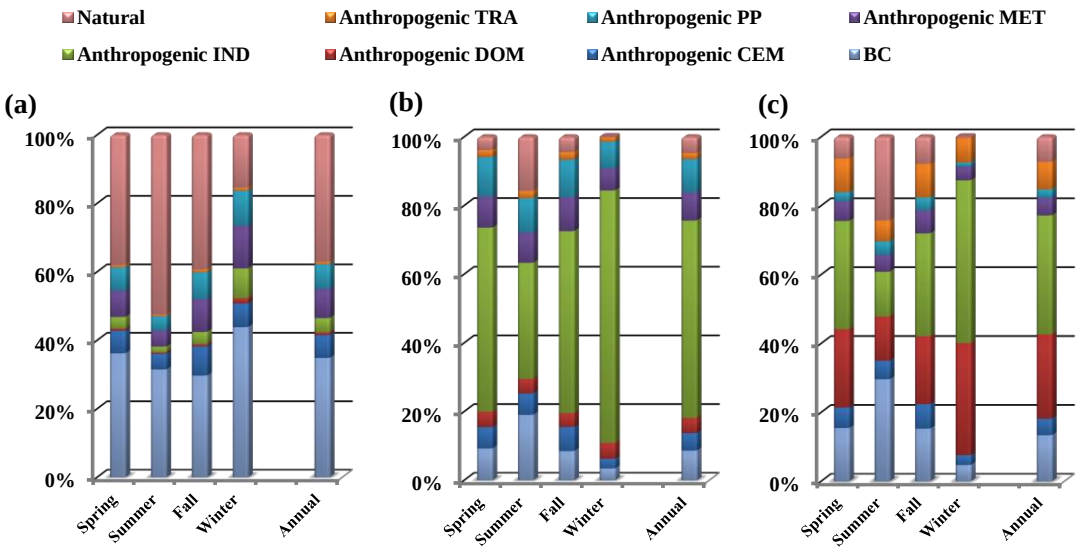

751

752 Figure 4 Source contributions to seasonal and annual averaged (a) GEM (b) GOM (c)

753 PBM concentration.

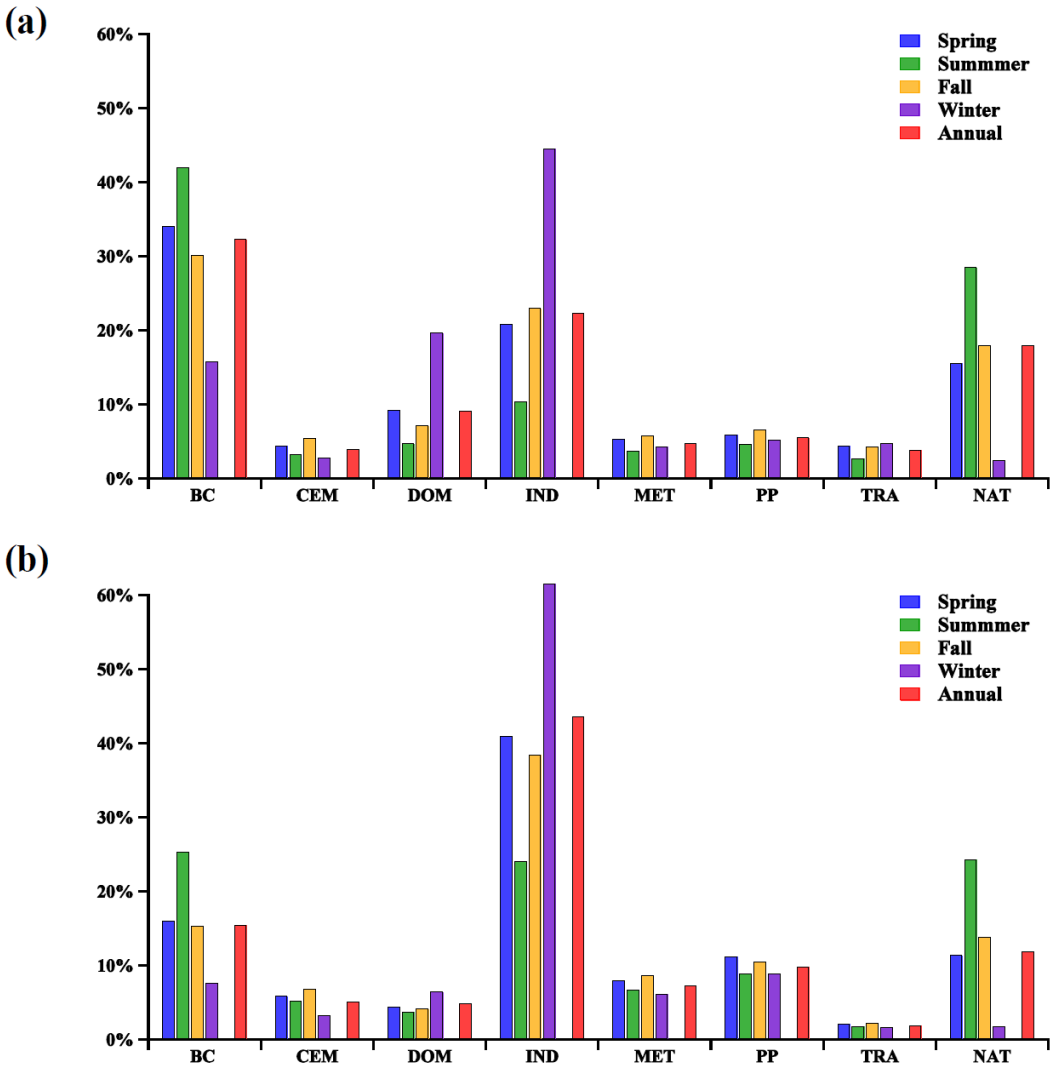

Figure 5 Source contributions to seasonal and annual mercury (a) wet and (b) dry deposition

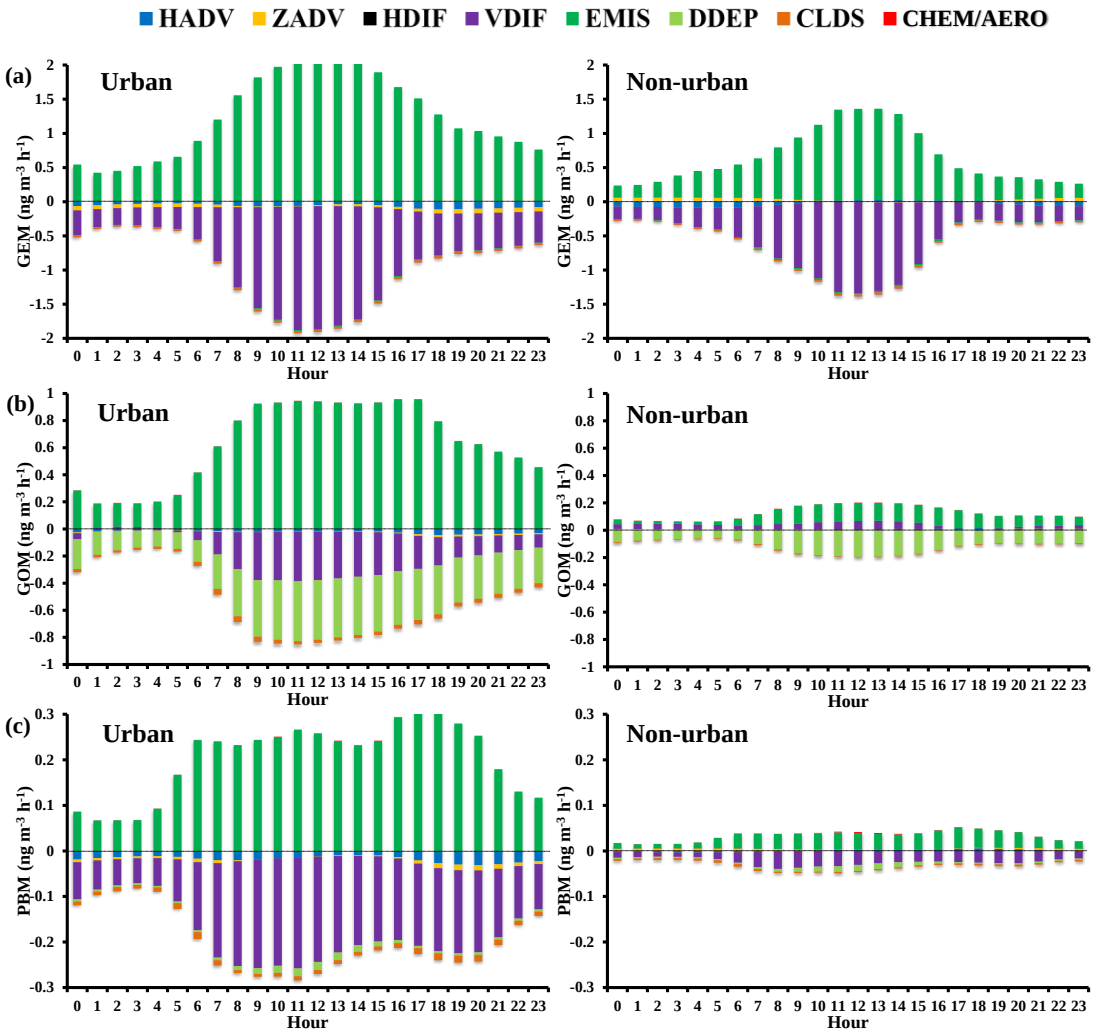

758

759 Figure 6 Diurnal variations of processes of (a) GEM, (b) GOM and (c) PBM in urban

760 and non-urban area.

761

762

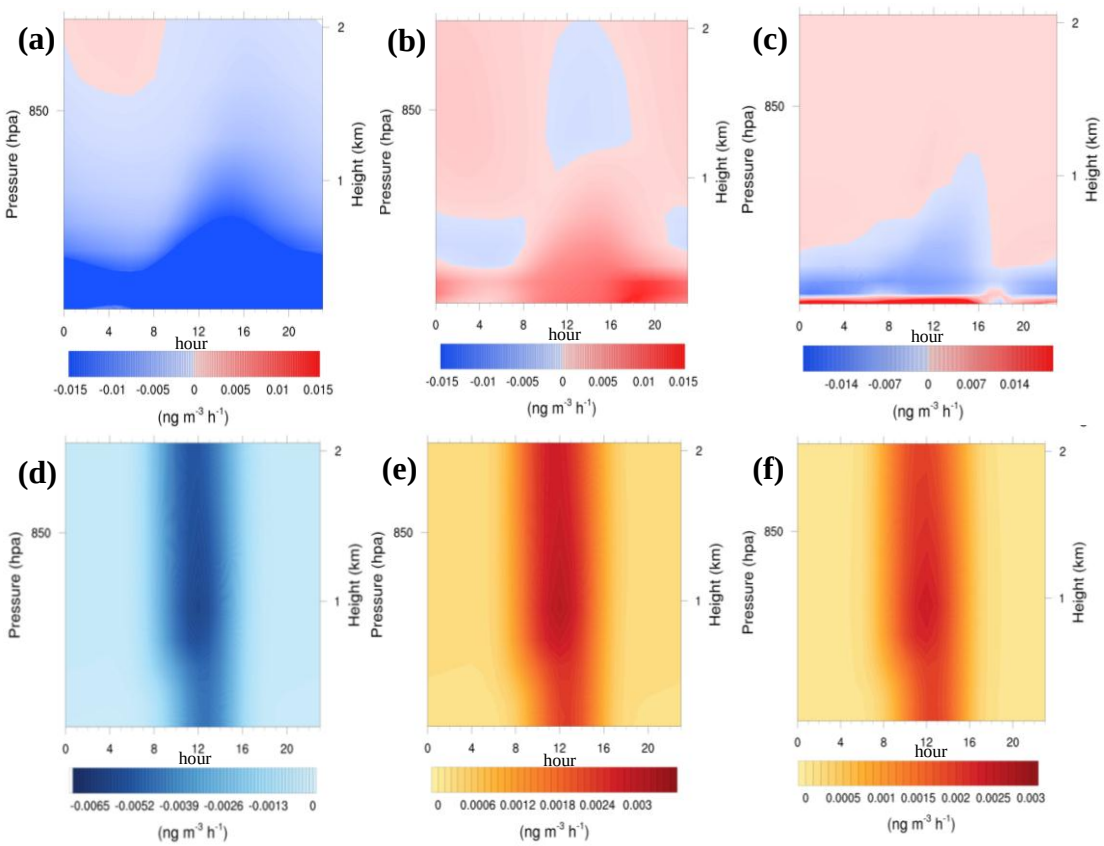

763

764 Figure 7 Profile of the contribution of (a) HADV to GOM in urban area and (b)

765 HADV to GOM, (c) VDIF to GOM, (d) CHEM to GEM, (e) CHEM to GOM, (f)

766 AERO to PBM in non-urban area.

767

768

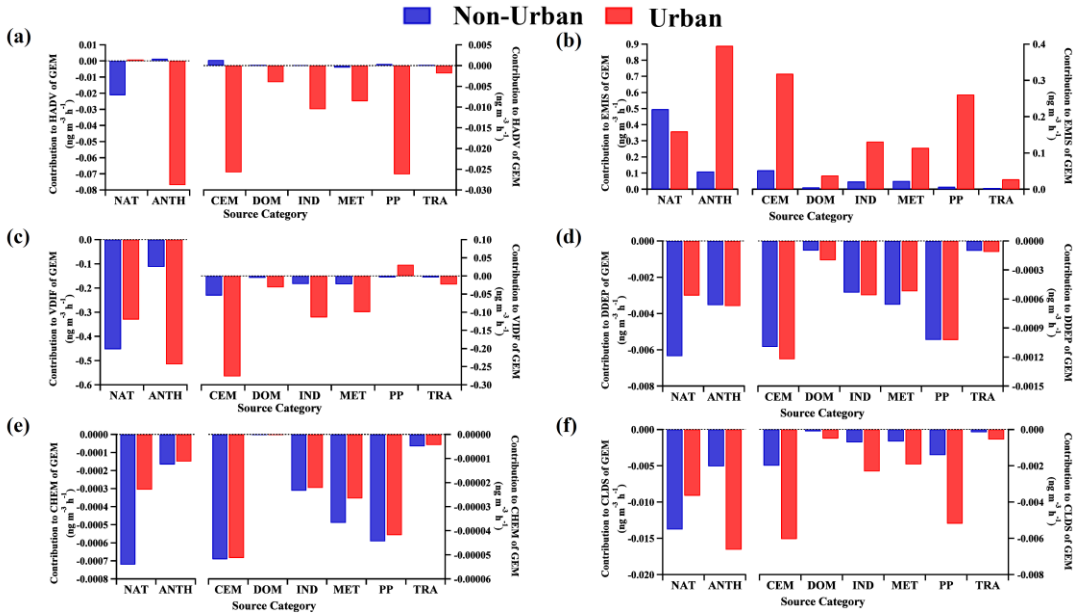

769

770 Figure 8 Impact of emission sources on (a) HADV, (b) EMIS, (c) VDIF, (d) DDEP, (e)

771 CHEM and (f) CLDS processes of GEM

772

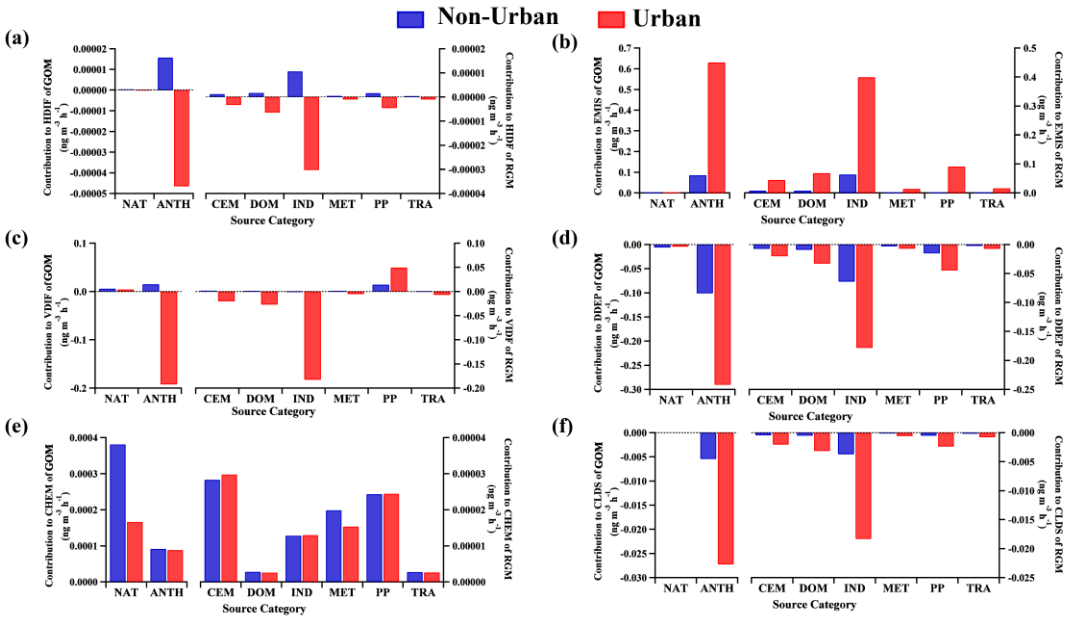

773

774 Figure 9 Impact of emission sources on (a) HADV, (b) EMIS, (c) VDIF, (d) DDEP, (e)

775 CHEM and (f) CLDS processes of GOM

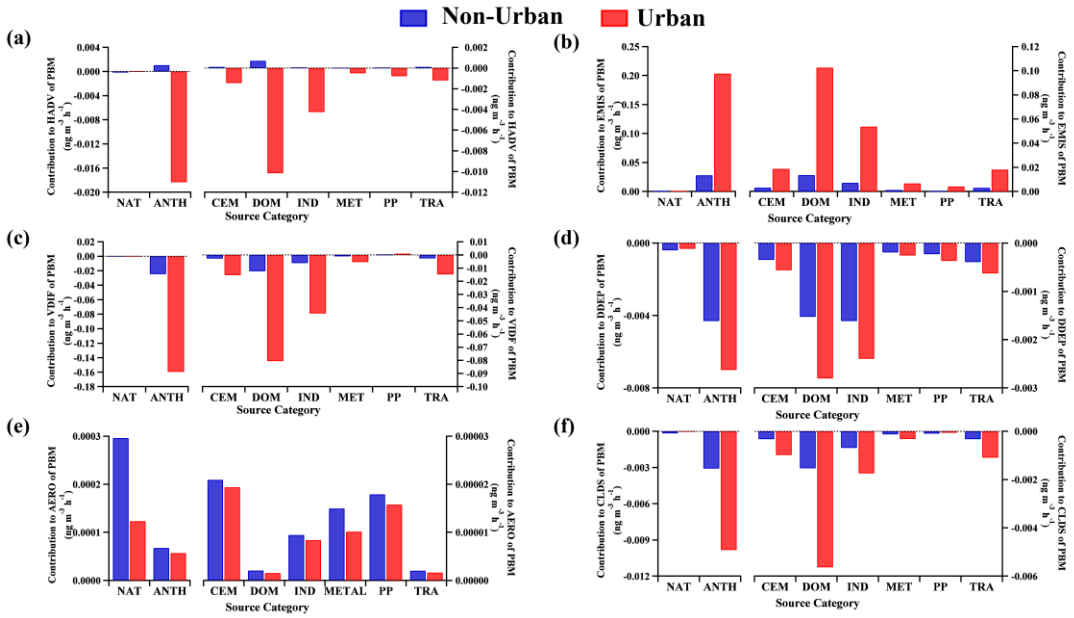

Figure 10 Impact of emission sources on (a) HADV, (b) EMIS, (c) VDIF, (d) DDEP, (e) CHEM and (f) CLDS processes of PBM